Tectonophysics 692 (2016) 152–163

Contents lists available at ScienceDirect

Tectonophysics

journal homepage: www.elsevier.com/locate/tecto

Dense network, intense seismicity and tectonics of Taiwan

Francis T. Wu [a,b,*], Zachary E. Ross [b], David Okaya [b], Yehuda Ben-Zion [b], Chien-Ying Wang [c], Hao Kuo-Chen [c], Wen-Tzong Liang [d]

[a] State University of New York at Binghamton, NY 13902, United States
[b] University of Southern California, Los Angeles, CA 90007, United States
[c] National Central University, Chungli, Taiwan
[d] Institute of Earth Sciences, Academia Sinica, Nankang, Taipei, Taiwan

ARTICLE INFO

Article history:
Received 6 April 2015
Received in revised form 19 March 2016
Accepted 13 April 2016
Available online 16 April 2016

Keywords:
Dense seismic array
Auto-picking
Relocation
Seismicity
Taiwan tectonics

ABSTRACT

A temporary seismic network consisting of 295 land stations was deployed in 2009 in Taiwan to monitor airgun sources during an onshore-offshore experiment in Taiwan. We exploit the continuously recorded dataset to detect and map seismicity in the seismically very active Taiwan. By combining recent automatic detection and phase picking techniques, we successfully generate an initial earthquake catalog of over 8400 events. The hypoDD algorithm is used to relocate and filter these events. This network recorded smaller events than the permanent regional network because of the many stations around the high mountain ranges and the generally high station density along 6 lines. The results based on the 2009 data generally reproduce the dominant seismicity features from many years of earthquake monitoring in Taiwan. In addition, we map hitherto unknown dipping zones under the Foothills and the Central Range that may correspond to seismogenic structures.

1. Introduction

Taiwan is a very young and active mountain building area where the Central Range (Figs. 1 and 2) is rapidly exhuming (Lee et al., 2006). High seismicity accompanies the geological processes and provides clues to the strain changes, material properties and the causative plate tectonic environment. Dense station coverage and abundant seismicity are both desirable for delineating active zones and their overall relations to the tectonic processes of a region. During the recent TAIGER project (Wu et al., 2014) stations monitoring airgun shots from R/V Langseth around Taiwan were deployed. In the more traditional "onshore–offshore" deployment, whose primary purpose was to record shipboard airguns, recording windows were set up. The 3-component instruments employed had sufficient data storage for continuous recording during the two and half months of the ship operation. The network included 295 stations along four nearly E–W transects at 2 km intervals (2009-03-18–2009-05-31) and two island-parallel lines at about 5 km intervals (2009-01-06–2009-06-24); sixteen stations in the network use broadband sensors and mostly occupied the same sites as our stations and they are not used in our analysis. Although not optimal for unbiased island-wide seismicity, the stations along the linear arrays are denser along the linear arrays compared to the permanent monitoring networks in Taiwan (e.g., Wang and Shin, 1998); many of the stations are located in areas not well covered by the permanent network. During the deployment a large number of $0 < M < 5$ events in and around Taiwan were recorded. The data are archived in an Antelope system (webpage — http://www.brtt.com/software.html). Manual picking of the dataset would be quite labor intensive and the picking of S arrivals can be difficult and inconsistent. We melded methodologies in Antelope database and recently developed for auto-picking of both P and S waves to streamline this process. Combining Antelope's automatic event association with recently developed P and S polarization pickers, more than 8000 events were initially identified and located. We relocated all events with the hypoDD algorithm (Waldhauser and Ellsworth, 2000) and found that many of the prominent features determined in previous studies using multi-year Central Weather Bureau (CWB) catalogs (e.g., Wu et al., 2004) are identified in our results. But some of the features in our results have not been previously observed.

Although the dataset was acquired mainly for the onshore-offshore study, with dense linear arrays surrounding the Central Range, an area not well covered by permanent stations, we wish to explore for new seismicity. This is a large enough dataset that manual phase picking is not practical and with the possible number of events recorded it becomes a challenge for auto-picking especially when we must pick S-waves both for location and for follow-up studies. We found that by coupling automatic detection and picking with careful relocation the problematic events can be efficiently and effectively filtered out. The locally dense stations produced patterns of seismicity in some regions,

* Corresponding author at: State University of New York at Binghamton, NY 13902, United States.
E-mail address: wu@binghamton.edu (F.T. Wu).

http://dx.doi.org/10.1016/j.tecto.2016.04.025
0040-1951/

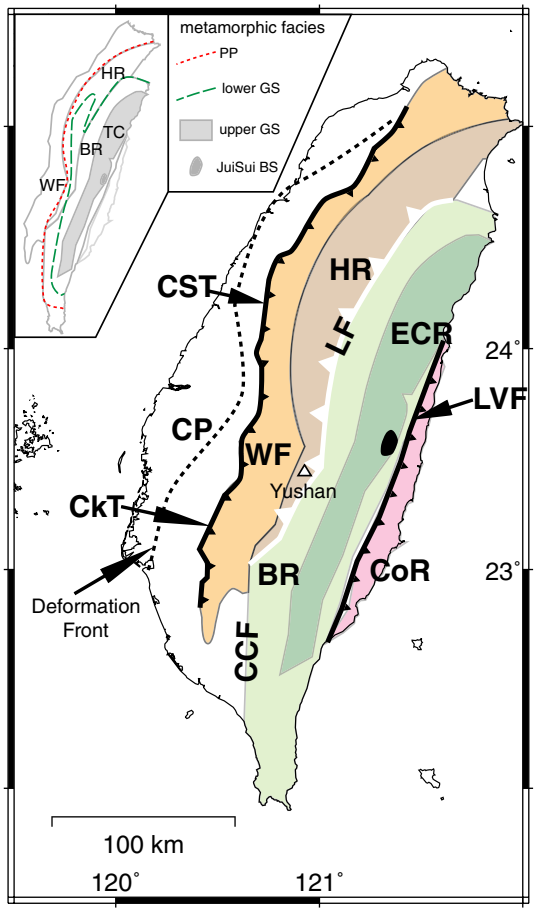

Fig. 1. Geologic framework and location map of Taiwan. CP = Coastal Plain, HR = Hsueshan Range, WF = Western Foothills, BR = Backbone Range, ECR = East Central Range, CoR = Coastal Range, CST = Chelunpu-Sanyi fault, CkT = Chouko fault (CST and CkT are representative mountain-front faults in western Taiwan), LF = Lishan Fault, CCF = Chauchou Fault, dashed line = deformation front, the assumed westernmost thrust. PP: Prehnite-Pumpellyite; GS: Greenschist; BS: Blueschist.

especially the Central Range and along the Central Taiwan transect, that had not been identified before and may be tectonically significant.

2. Seismic network and data

The data used in this study were acquired in 2009 during the onshore-offshore phase of the TAIGER project in Taiwan (Wu et al., 2014). A total of 295 short-period stations were deployed along four main EW and two NS lines. The four nearly EW lines were the main "transects" of the TAIGER project along which stations were placed at 2 km intervals, access permitting (Fig. 3). These instruments were recording from 2009-03-18 to 2009-05-31. The two island-parallel lines, with a total of 77 stations, were in operation from 2009-01-06 to 2009-06-26 for improved lateral coverage of the mountainous areas. All channels of the instruments had a uniform sampling rate of 100 Hz. Most of the instruments were provided by IRIS/PASSCAL (http:iris.edu). Among the 295 stations used for this study all recorders were set in continuous recording mode so that both the shipboard air gun sources and natural earthquakes were recorded. With the exceptionally high seismicity rate in Taiwan a large amount of data was recorded, especially during the two and a half months from mid-March to the end of May when both the EW and NS lines were deployed. In general the quality of the recordings in the mountains are better than those in the Western Foothills or Coastal Plain. Earthquakes in the near offshore area in the east are particularly numerous. In this paper we will use the whole dataset from the automated picking processes to assess the performance of the temporary network.

3. Methodology

Due to the large amount of data available for our study and the wish to use objective algorithm for picking S-waves we decided to use automatic processing and locate all events from scratch. The methodology employed in this study begins with the raw continuous data. Although we have at our disposal the Taiwan CWB network local seismicity catalog for the period, with which we will compare later, the data processing began with detection of signals on all the continuous data available for the network. The procedure and workflow are integrated with the Antelope seismic database platform (Pavlis et al., 2004). We summarize the procedure briefly as follows: 1) run time series detectors to find transient signals (above our chosen signal to noise ratio) of interest, 2) modulate 3-component data using polarization filters to isolate P and S phases, 3) use STA/LTA for picking P and kurtosis detector to pick S, 4) associate these "signals" to P and S for preliminary event location, and 5) invert phases for hypocenter. Since the two procedures we adopt for this paper were applied separately for different purposes we shall give some details of how they are implemented for this dataset.

First, the earthquake detection algorithm of Ross and Ben-Zion (2014a) was applied to the vertical component for each station to identify transient signals of interest. As in most seismic signal detection techniques the sudden increase of a short time average (STA) of a time series against the background of the long time average is an effective means of detecting the start of a transient signal (Allen, 1982). Instead of using one ratio, Ross and Ben-Zion (ibid.) use a bank of 10 of them, with various window lengths and frequency bands, to form a more robust combined detector. Defined as the "pseudo-probability time series" (PPTS), the composite STA/LTA has built-in redundancy and is more sensitive. The parameters for the ten detectors were listed in Table 1 of Ross & Ben-Zion (ibid.) and the same detection thresholds were used here, i.e., a trigger window was initiated when a PPTS value of 0.3 was met on any trace, and turned off when the PPTS fell to 0.1. If the peak PPTS value during this window was less than 0.82, the window was discarded. If the peak value was larger than this threshold, then the trigger-on time was used to create a windowed 3-component (Z, N and E) set, starting 10 s prior and ending 30 s after (herein referred to as the data window) for the particular station.

In the windows of 3-component seismograms identified above a P-pick is made on the vertical and an S-pick on the horizontal components following the procedures of Ross and Ben-Zion (2014b). The key steps are as follows. P-waves are picked using an STA/LTA algorithm on P-polarized vertical traces. S-waves are initially picked using an STA/LTA algorithm on S-polarized horizontal traces, and the picks are then refined using kurtosis-based detectors and their derivatives (Saragiotis et al., 2002). Kurtosis, in arrival picking, is a measure that refers to the amplitude histogram within a certain time window (5 s); near the arrival of a wave it increases sharply as the variance remains nearly the same but the "tail" grows significantly and so does the kurtosis (Fig. 4). Additional details on the procedure are given in sections 2 and 3 of Ross and Ben-Zion (2014b). If successful S picks were made on both horizontal data windows, we chose the one with the largest signal to noise ratio. Applying both of the phase picking algorithms to the data windows provided roughly 3.7 million initial P- and S-wave detections from all components.

The next task was to associate detections with actual earthquakes. We performed the event association using a built-in procedure in the Antelope system. The event association is performed in two stages: 1) determine whether any set of P-detections back-project to a coherent source location within a pre-defined set of grids (Fig. 5), and 2) determine whether any of the companion S-detections back-project to the same origin. If detections were found to be associated with an event they were used as phase arrivals in a formal hypocenter inversion of

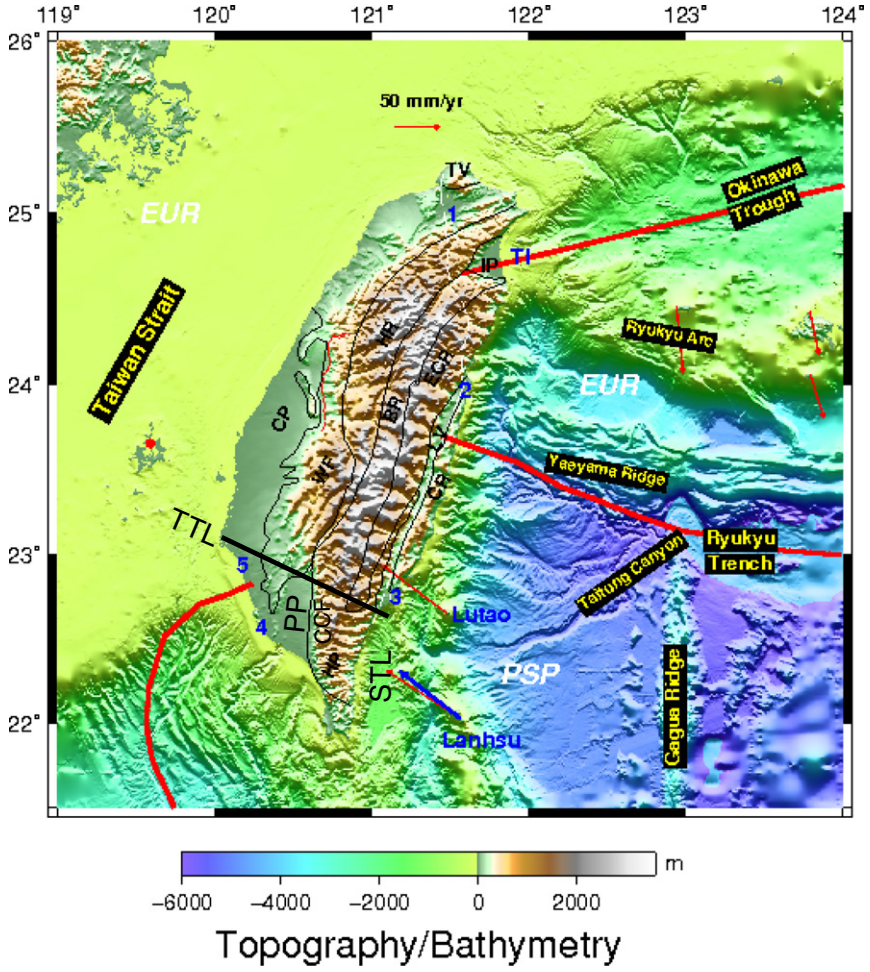

Fig. 2. Plate boundaries around Taiwan. Solid red line: subduction boundaries. Red line, the western edge of the subducted PSP. Red vectors: measured GPS velocity vectors, relative to the red circle in Penghu Island. Blue vector: PSP motion predicted by Seno et al. (1993). Geological units: DP = Coastal Plain, WF = Western Foothills, HR = Hsueshan Range, BR = Backbone Range, ECR = Eastern Central Range, TV = Tatun Volcanoes, IP = Ilan Plain and CR = Coastal Range. Cities: 1 = Taipei, 2 = Hualien, 3 = Taitung, 4 = Kaohsiung, and 5-Tainan. TTL = Tainan Taitung line. The Chelungpu fault that was activated during the 1999 Chi-Chi earthquake is shown in red to the right of "CP". Note BR and ECR are lumped together as Central Range.

P- and S-waves arrival times. For the back-projection stage we defined local and regional grids (Fig. 5) in order to locate events around Taiwan. The local grid had 151 nodes in the latitude and longitude directions, while the regional grid had 101 nodes in each direction. The local grid had depth slices spaced every 2 km from 0 to 30 km, and spaced 4 km from 30 to 90 km. The regional grid had depth slices every 10 km from 0 to 90 km. At this initial stage of the detection process, we used the IASPEI91 model of Kennett and Engdahl (1991) to calculate travel times — the choice of a particular model is not critical in this step.

A successful association is declared when a test event within a certain grid would generate arrival times of P-waves within a certain time window of a set of picks (set at 1.5 s). We require a minimum of 9 P-wave picks to fall within the time window for origins within 50 km of the furthest receiver, and a minimum of 11 P-wave picks beyond this distance. The number was chosen based on extensive testing of the Antelope associator on other large station datasets, such as the AZ network in Southern California (F. Vernon, personal comm.), as well as considerable testing of the TAIGER dataset itself. S-wave picks are not explicitly required in the detection process because the P-wave picks are more frequent and more robust, however they are included in the location process when present. When a successful association occurred the location of the grid node was used as a trial location. All phase arrival picks associated with this event were then submitted to the GENLOC algorithm of Pavlis et al. (2004) to invert formally for an earthquake hypocenter. The seismograms for each located event were lastly converted to Wood-Anderson equivalent and a local magnitude M_L was computed. The epicenters in Fig. 6 are shown with the magnitudes color-coded; we note that small events (dark brown) appear near the stations and many larger events are located offshore of eastern Taiwan.

4. Analysis of earthquake locations

The procedure adopted above produced 8444 earthquakes associated with 339,000 P-picks and 132,000 S-picks. We inspected approximately 2000 of these events at each of the 295 stations and found that the detections were genuine and the phase picks were reliable. The hypocenters shown in Fig. 7a show a significant number of deep (red dots with depth ~100 km) events. A series of cross sections nearly perpendicular to the island (Fig. 7b) show that the seismicity follows the main seismic zones identified in many previous studies. For example, under the southern Coastal Range a clear east-dipping zone (Fig. 7b profiles 12–14 near the 100 km mark) an east-dipping seismic zone has been identified with an earthquake fault (Kuochen et al., 2007). But in both the map view and these sections the hypocenters scatter noticeably more (cf. Wu et al., 2004) and there are many events deeper than about 40 km under the island, exceeding the known depths of well constrained hypocenters, especially under the Central Range (Wu et al., 2014). The stations used in this study are confined to the land area and the apertures of the mainly linear arrays are not optimal for

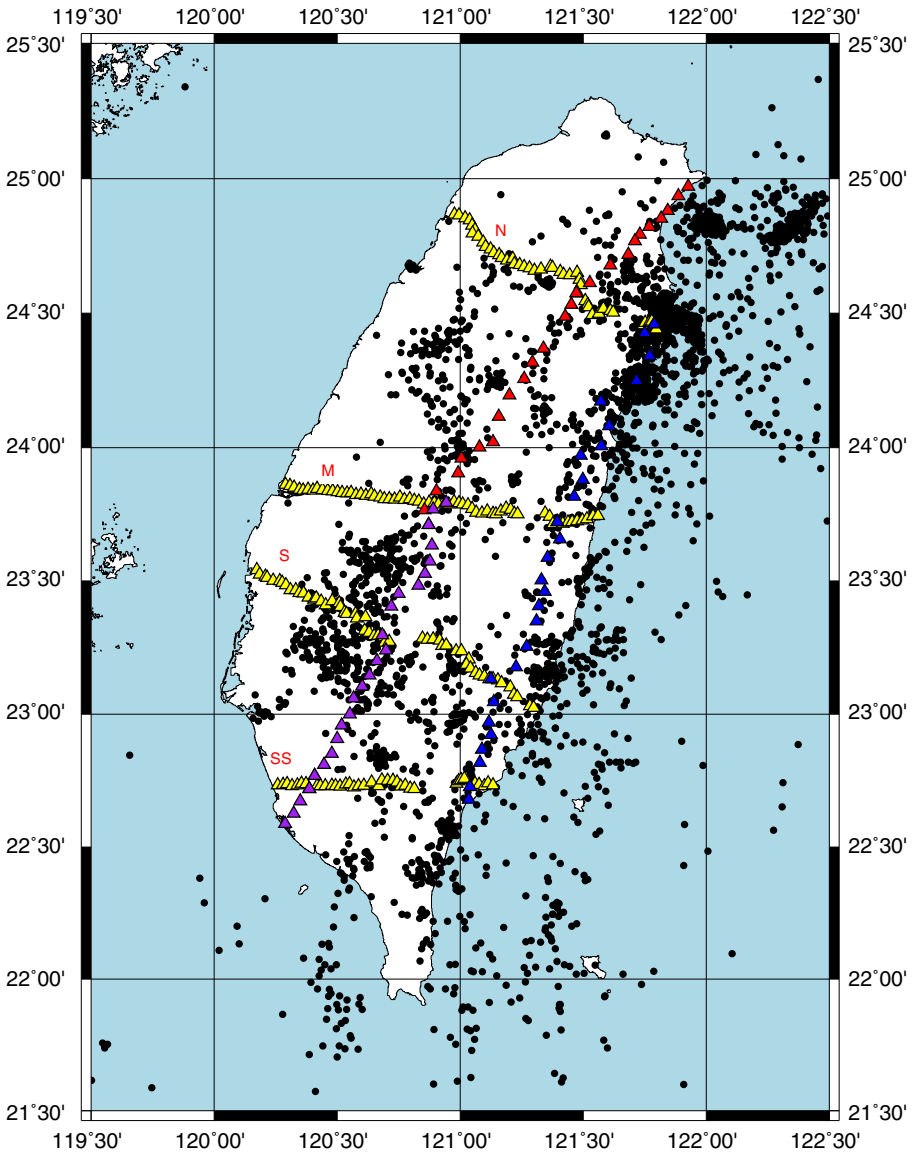

Fig. 3. Sea-land network stations (triangles) and CWB catalog events during the period of operation. The red, blue, and purple triangles correspond to the NSN, NSE, and NSS lines respectively. The EW lines are the main transects of TAIGER: N: northern line, M: middle line, S: southern line and SS: Hengchun Peninsula line.

events offshore to the east or the west of the island (Fig. 3). The availability of S-picks does help to constrain the offshore locations, and the resolution of the eastern near shore events are made possible as a result.

To investigate whether the large database of P- and S- picks and their associated events can shed more light on the spatial distribution of small magnitude events and whether any new structures are illuminated by the seismicity we relocate the events using the well-known hypoDD algorithm (Waldhauser and Ellsworth, 2000). We used a 1D velocity model for the Taiwan region established by the Central Weather Bureau of Taiwan in their routine earthquake location (Shin and Chen, 1988). The hypoDD algorithm places the 8444 events into many clusters in which event chains were formed, but the first one has 6511 events and the others have 12 or less. For this cluster a total of 389,637 P and 168,660 S differences ("dtimes") were chosen. We let the relocation go through 6 group of iteration parameters for a total of 30 iterations with successively tighter specifications for correlation distance (varying form 12 km to 4 km (20–30th) and smaller damping (from 100 to 50). At the 20th iteration, the results (totaling 4863) show clustered events both in map view and in cross sections (Fig. 8a and b). Fig. 9 shows the locations of the events not relocated at this stage and it is clear that all events in the Taiwan Strait and most of the events below a depth of about 40 km have been eliminated because they do not satisfy the requirements for hypoDD relocation; the additional factor is that stations in the Coastal Plain have much higher noise level, resulting in fewer picks for those events. The events offshore of eastern Taiwan were relocated for larger events with an abundance of S and P arrivals. At the 30th iteration the clustering is more evident (Fig. 10). Many well-delineated zones are defined quite clearly and several new features are defined in addition. To avoid repetition they will be described in the following section.

Although in hypoDD relocation station "gap", i.e., the azimuthal station coverage is important as is in traditional location method, the organization of arrival times for different events into networked data improve the convergence process. We show the convergence curves and the network configuration (showing the azimuth and distance of stations with the event at the center — each division along the radial axis is 20 km) for four events (Fig. 11). We see that even when the recording stations lie along a line the convergence could be quite rapid. In general, events with stations all around the events have smoother and monotonically decreasing convergence curves.

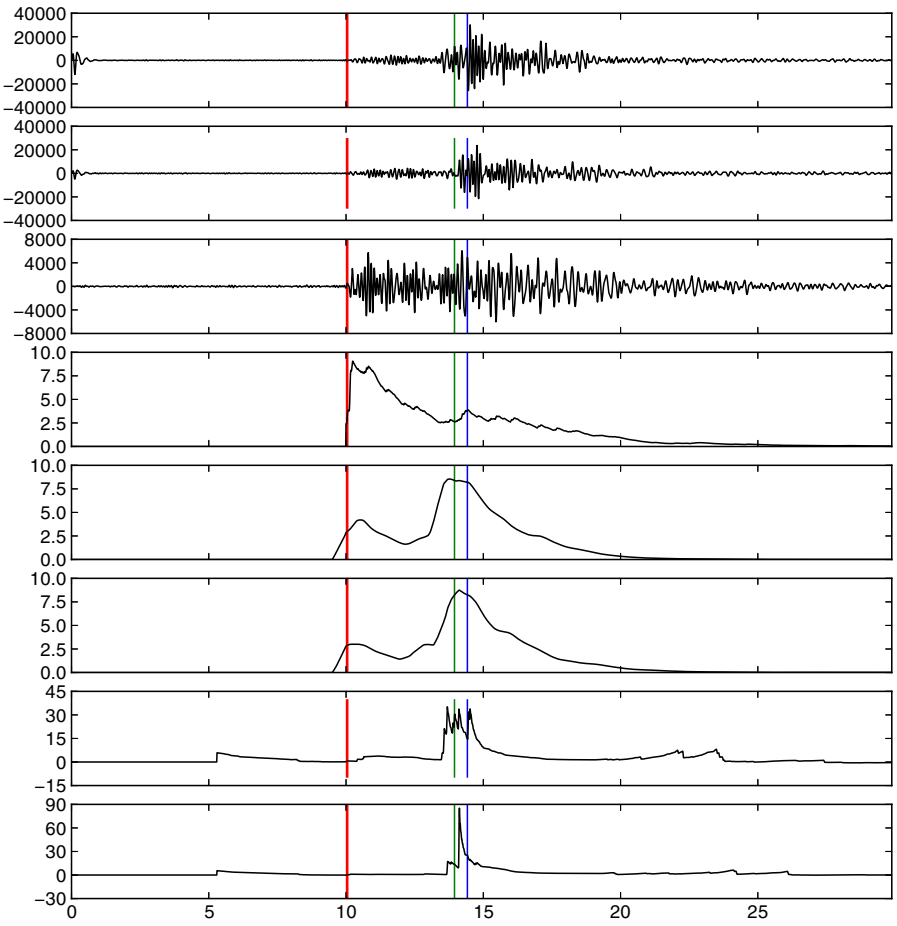

Fig. 4. Cartoon summarizing the picking processes for P and S waves: a time-series detector is first calculated on each vertical component trace to identify approximate start times of transient signals of interest (stars). For each transient signal identified, P-wave picks are attempted on vertical components (Z), and S-wave picks are attempted on both horizontal components (H). Here the picks are indicated by arrows on the respective component. When enough picks accumulate in a window of time, the travel times from each receiver to a trial source location are subtracted from the respective pick. When a sufficient number of migrated picks cluster in a pre-defined time window (shaded region), an event is detected.

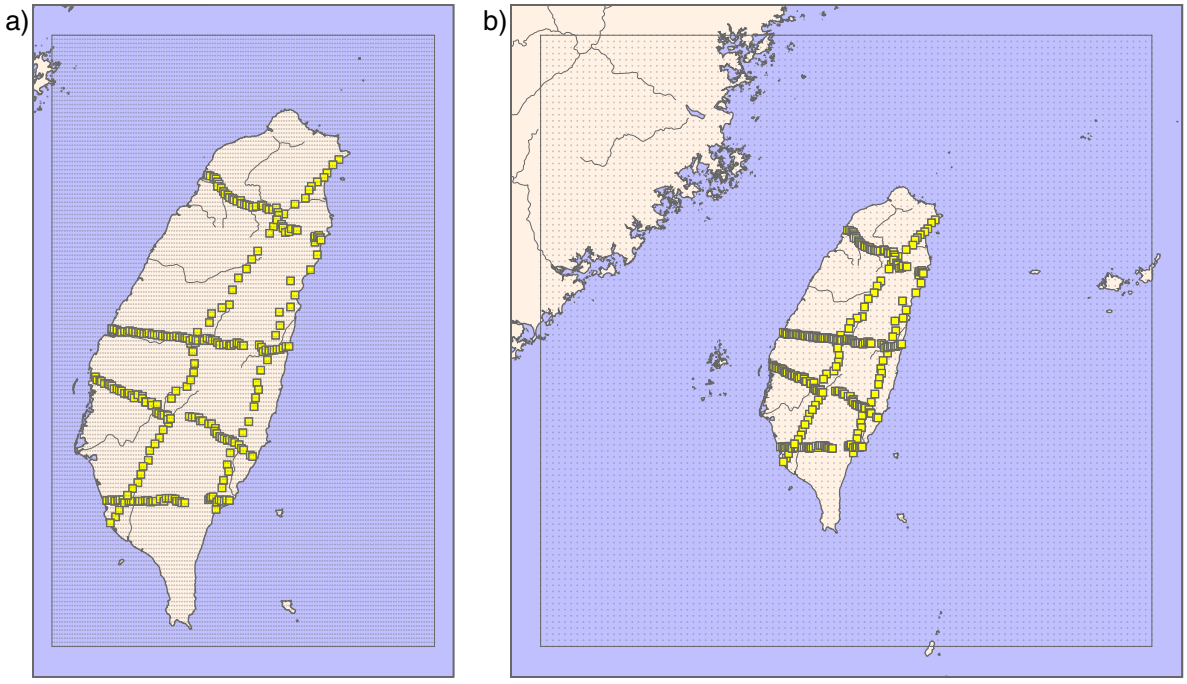

Fig. 5. Grids used for association of phase detections with coherent source origins. The yellow squares indicate TAIGER stations. a) Local event grid consisting of 151 × 151 nodes in the horizontal dimensions. b) Regional event grid consisting of 101 × 101 nodes in the horizontal dimensions.

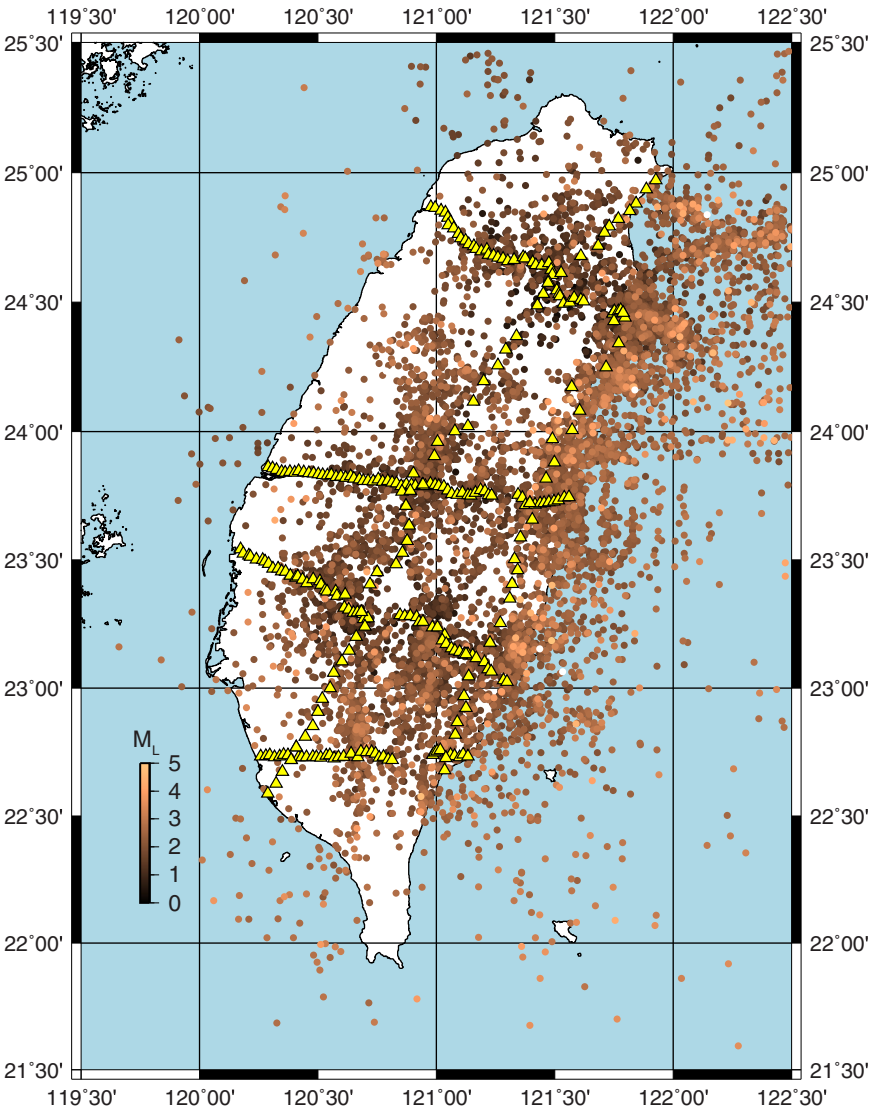

Fig. 6. Results of the detection process for the complete database. Over 8400 earthquakes were detected (colored circles) by the 295 stations (yellow triangles). These locations are the preliminary hypocenters from the detection/location process, before any relocation is done with HypoDD. The largest magnitude events tend to be located on the northeast side of the island, and offshore.

5. Comparisons with CWB catalog

To gain some perspective how our network performs we can compare the results obtained in this study with those of the permanent Taiwanese seismic network operated by the Central Weather Bureau (CWB), especially with relocation results of Wu et al. (2004). Although there are networks of different sensors and upgraded in 2010 to include many new stations, the pre-2010 CWB seismicity catalogs are based on a network of ~80 short period seismic stations, with an average spacing of about 15–20 km, including stations offshore of southeast Taiwan, in the Strait, and on the southeastern Chinese shore. In recent years picks from the islands at the end of Ryukyu chains are also utilized. In the 2009 CWB catalog located 3315 earthquakes from 2009-03-20 to 2009-05-31 (Fig. 3) using manual phase picking. A large number of events in the Taiwan Strait, offshore of SE and NE Taiwan are included. The TAIGER sealand network had roughly three times as many stations in operation as the CWB did during the common time period, and Fig. 3 shows that between 22.7 and 24.3 latitudes our stations surround the Central Range and many stations are located in the Central Range itself. The TAIGER network should be expected to be better suited for locating well recorded earthquakes in the regions surrounded by its arrays and, in addition, detecting smaller earthquakes near dense stations.

Fig. 12a and b shows frequency-magnitude distributions for both networks (total 3315 CWB vs 8444 TAIGER events) during the common time period. The distributions are similar in shape, with more TAIGER network events in all magnitude ranges. Some of the largest differences between the two catalogs are in the range of M_L 1–1.5, where the TAIGER catalog contains between 2–3 times as many events. A number of offshore events make up the two catalogs. Taiwan is one of the most seismically active regions in the world, as evidenced by the 300+ events with $M_L > 3$ detected during a period with no major earthquake in the region. This unusually high seismicity rate (~90 events per day) renders the automatic picking appropriate. For the overlapping events in the CWB and the 20th iteration catalogs, we show the relation between their magnitudes (Fig. 12c); the two generally track each other with our values half a magnitude higher around our M_L 5. The dense TAIGER stations facilitated recording more small events near them. On the flip side, the TAIGER network mislocated a number of offshore small events as being under the island or at lower crustal or upper mantle depths initially and these were eliminated in the relocation. The

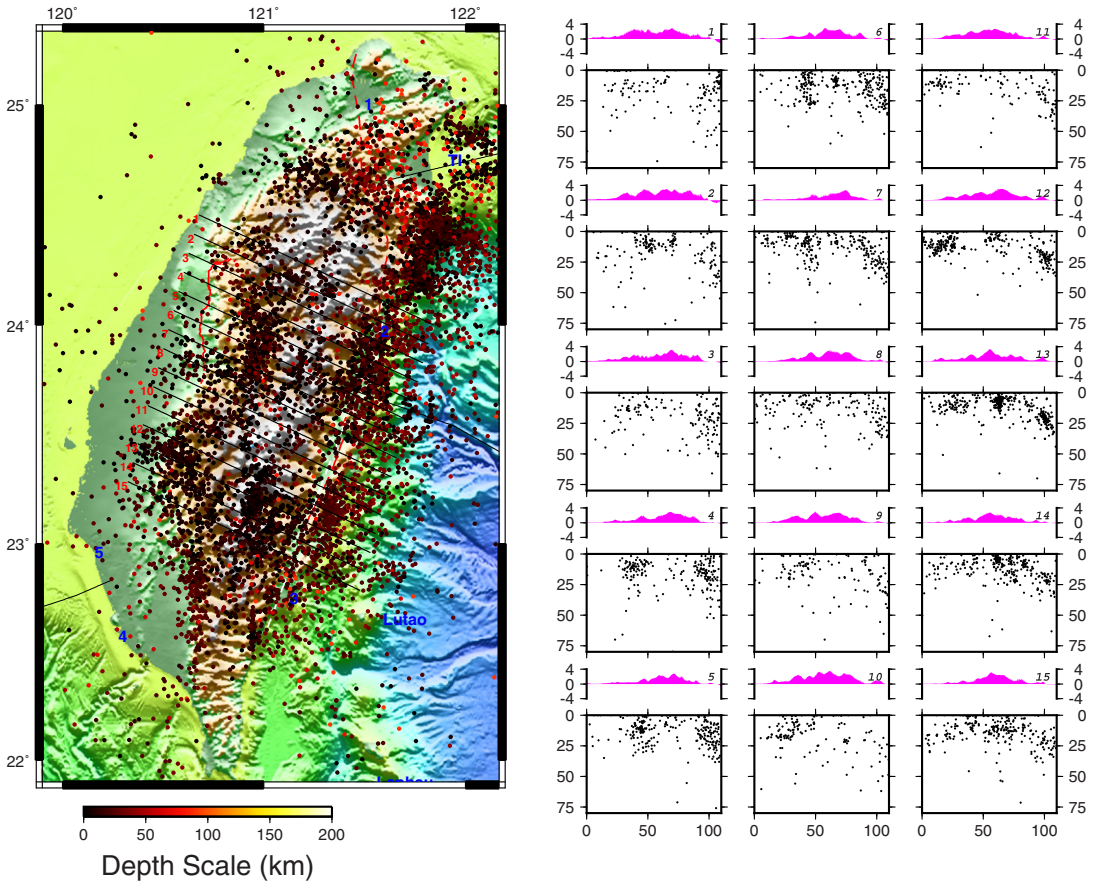

Fig. 7. All events (8444) located by the initial automatic processing. (a) Epicentral distribution and (b) seismicity profiles across Central Taiwan. As in all profiles the pink shaded regions above the seismicity indicate the elevation along-profile.

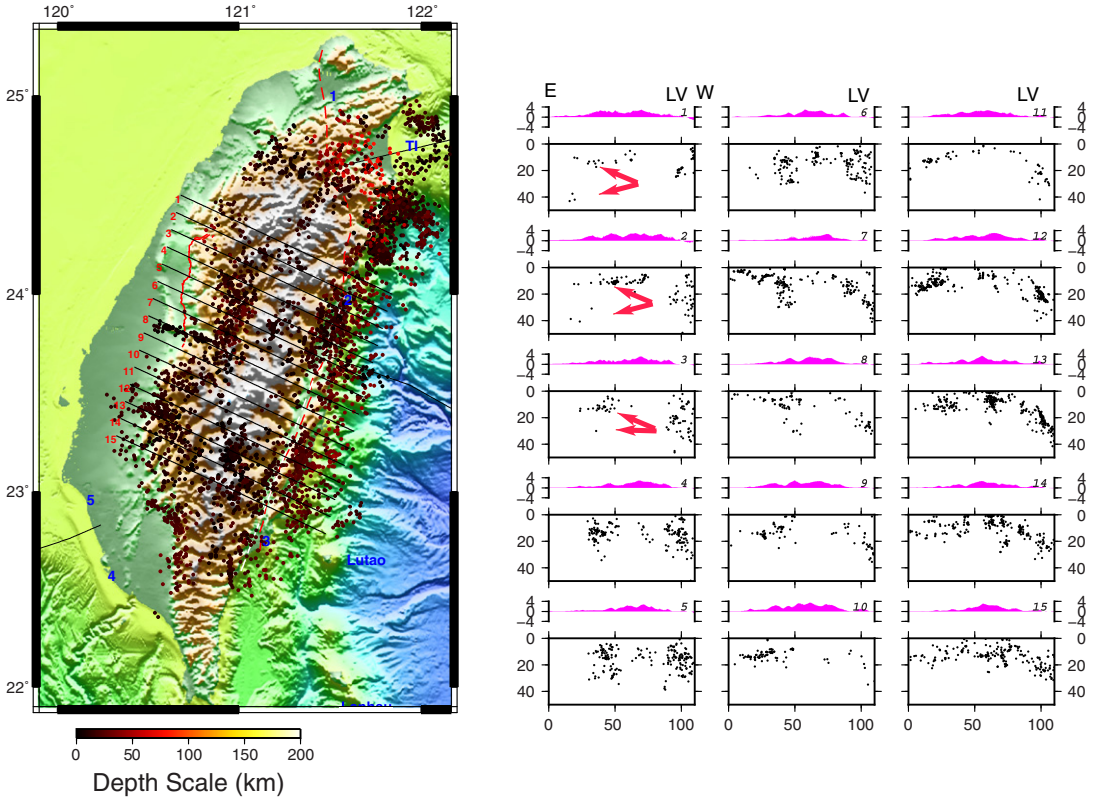

Fig. 8. Results of 20th iteration in hypoDD relocation. (left) Map of epicentral distribution and (right) seismicity sections across Central Taiwan — profile locations shown in map. The pink shaded regions indicate the elevation along-profile.

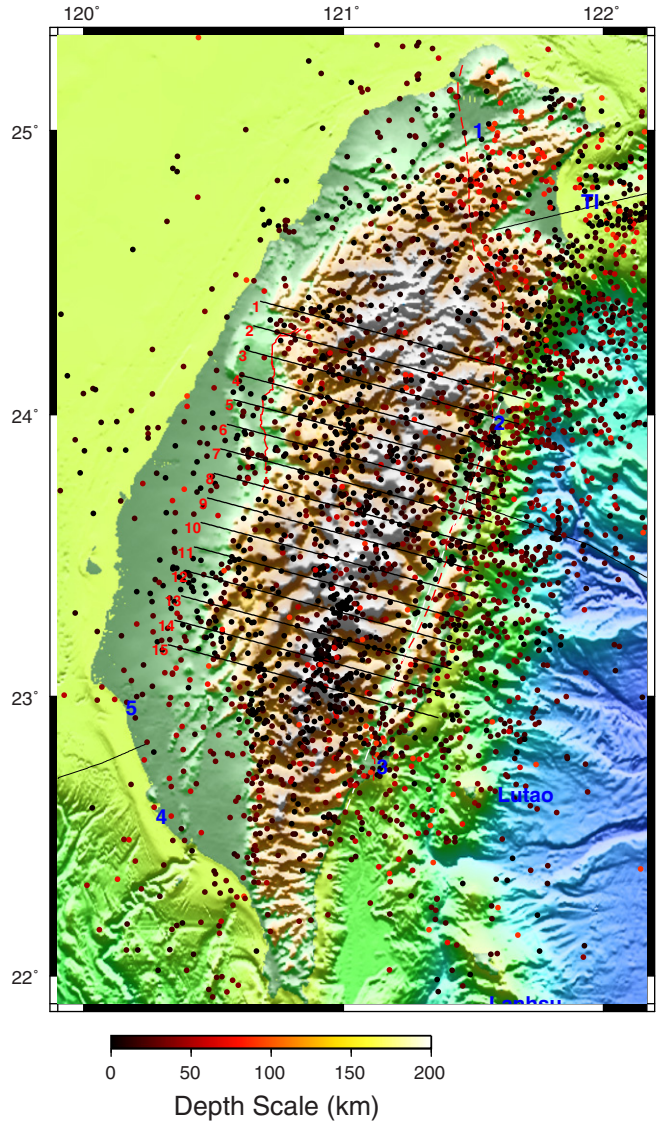

Fig. 9. From a starting set of 8444 events 4863 were relocated in the 20th iteration. Here the events left out at this stage are shown in the map. The events left out consist generally of offshore events on all sides of Taiwan, and many deep events (below 40 km under the Central Range and Foothills). See text for explanation.

histograms (Fig. 12d and e) compare events that are only common between the 20th iteration hypoDD results and the CWB catalog. There are 1900 events common in total. The red lines indicate the Gutenberg-Richter distribution, while the black lines describe the cumulative Gutenberg-Richter distribution. The dashed blue line provides an estimate for the completeness magnitude of each dataset. In the next plot, ML values are compared on an event basis between the two catalogs. The ML values for the Sea-land dataset are on average 0.22 units larger than the ML values for the CWB dataset. The ML software used is the part of the standard Antelope package, and the way that the CWB calculates ML may differ. It is also expected that the larger events, which are generally offshore or on the edges of the network, are less well constrained due to the network geometry. This may have an effect of slightly increasing the average magnitude as well.

The locations of the two networks are mostly within 0.1 degree in longitude or latitude (Fig. 13). Finally, in Fig. 14a we show the differences in the locations of the TAIGER and CWB networks. With the circle at the TAIGER location and the line segment indicating the offset of the CWB location, many events are within a short distance from each other, although offshore events appear to have large offsets. In Fig. 14b the events located by the TAIGER, but not the CWB, network is shown; the many small events near the network arrays dominate for obvious reasons. In Fig. 14c, the events recorded by the CWB, but not TAIGER, network are shown; not including the more distant offshore eastern or southern Taiwan events in the TAIGER catalog is understandable. Missing the relatively small events by the TAIGER linear arrays in southwestern Taiwan events can be understood in terms of the presence of comparatively dense CWB stations in the area.

6. Discussion and conclusions

6.1. Taiwan tectonics and its relation to seismicity

Taiwan has a length of about 400 km and a width of 135 km at its widest. The simple geology map (Fig. 1) shows the main structural units and the faults. The topography and the plate boundaries are shown in Fig. 2 (also see Wu et al., 2014). A cross-section from west to east in the mid-section (about 23.5°N) of Taiwan encounters first the Coastal Plain (CP). It is underlain by earlier Pliocene and older sediments supplied from the mainland and Pliocene to recent sediments from the east, as the mountains rose from sea level. Toward the east the Western Foothills (WF) rises above the plain to elevations exceeding 2000 m. Further east the Central Range (CR), often divided into the Backbone Range (BR) and Eastern Central Range (ECR) as shown in Fig. 1, soars up to almost 4000 m at the highest, and is cored by Mesozoic or earlier metamorphic rocks. This Range is bounded on the east by a long, somewhat linear feature of roughly 10 km wide, the Longitudinal Valley (LV). East of this Valley is the Coastal Range (CoR), composed of materials from the arc complex and sits on the edge of the Philippine Sea plate (PSP). If a section is taken 20 km to the north of 23.5°N, say, then another range is interposed between WF and CR, the Hsueshan Range, composed of Paleocene shelf sediments. The mid-section of Taiwan is generally explained as the result of arc–continent collision, with LV as the main contact between PSP and the Eurasian Continent (EUP). The overall plate configuration of the area is shown in Fig. 2 (Wu et al., 2014). How exactly the collision produced the mountains is still being discussed. Being an active and young orogen, the locations and focal mechanisms of earthquakes provide key sources of information inside the mountains where the deformation takes place.

Some of the major geologic boundaries in Figs. 1 and 2 are major faults. For example the CST (Fig. 1) was the main fault in the 1999 M7.6 Chi-Chi earthquake; in the LV the Longitudinal Valley Fault (LVF) is thought to be associated with two M7 + earthquakes in 1951. Recently Kuo-Chen et al. (2015) have raised the question of whether the major stratigraphic boundary between the Central Range and the Hsueshan Range is active. CkT and CCF (Fig. 1) have not yet had a significant event along them.

In the young and rapidly exhuming Taiwan orogen the materials apparently undergo both brittle and ductile deformation. Earthquakes represent brittle deformation and they form an integral part of the study of this modern orogeny. Since seismicity is episodic and our total record of seismicity is relatively short we need to exploit all available datasets and this study shows our attempt to use an unusual seismic data source and auto-picking for this purpose.

6.2. Auto-picking, seismicity and tectonics

Although the recording of earthquakes was not the primary purpose of the linear arrays deployed during the March–May, 2009, the continuous time series produced results that add to the existing knowledge of seismicity of Taiwan. In locating the events we demonstrated the efficacy of using auto-picking techniques on a massive dataset; coupled with hypoDD relocation we obtained an independent catalog rivaling that of a permanent network. Being our first attempt to process such a large dataset, a few trials were needed to finalize our results by applying previously tested picking procedures,

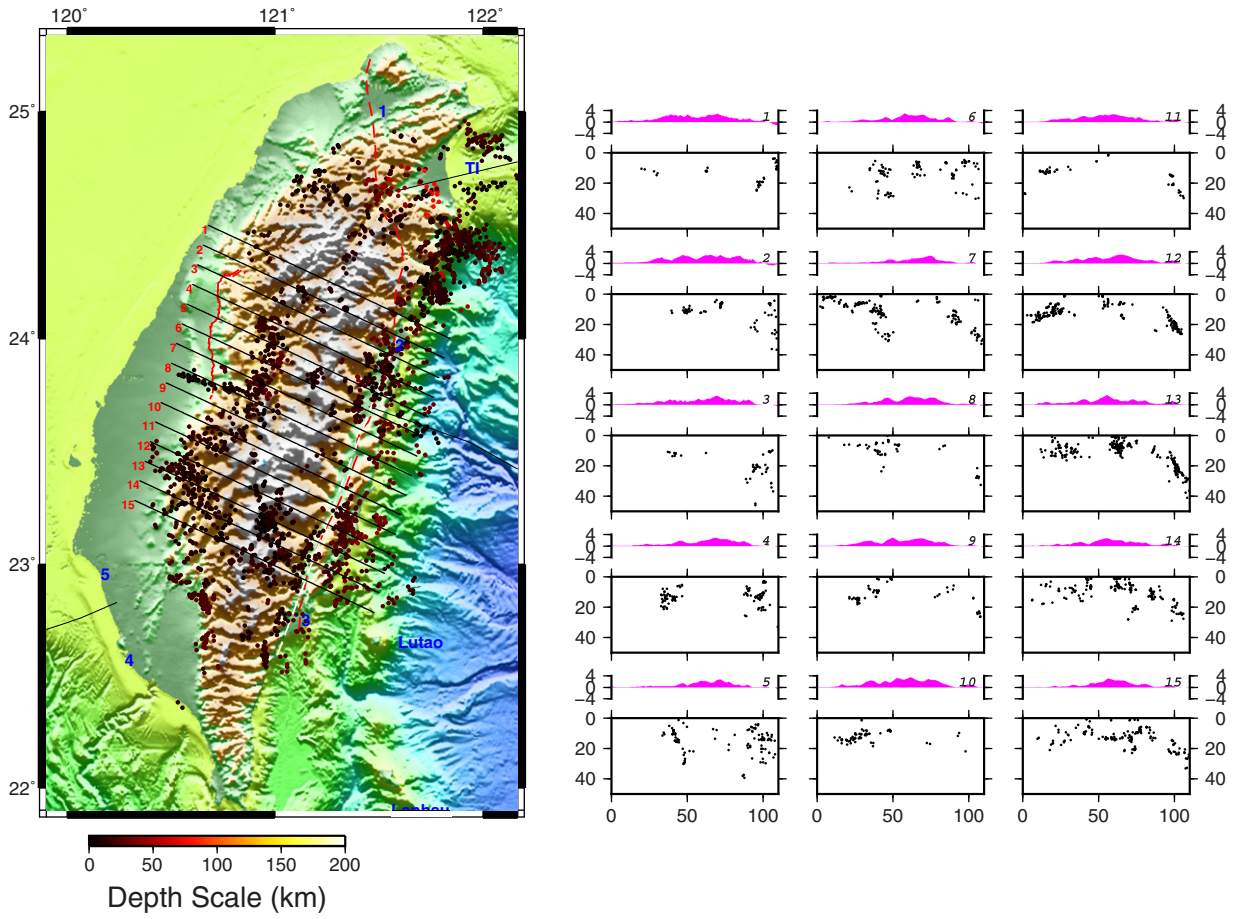

Fig. 10. Results of the 30th iteration of hypoDD relocation. (left) Map of epicentral distribution and (right) seismicity sections across Central Taiwan — profile locations shown in map. See text for explanation.

This study was possible because Taiwan has a high level of seismicity related to the active collision-related orogeny. Large earthquakes have caused significant damage since 1650, when the systematic historical record-keeping began. The largest event on land appears to be the 1999 Chi-Chi earthquake; the causative fault is a reverse fault and lies under the Western Foothills. Mapping of seismicity improved throughout the 20th century and the fact that the seismicity is evidently related closely to the active orogeny and to rheology (Wu et al., 1997, 2004; Kim et al., 2005) makes detailed seismicity study an important scientific problem. Even though our main deployment covers less than three months, most of the main features in seismicity can be discerned — a more thorough discussion of seismicity and tectonics can be found in Wu et al. (2014).

Figs. 8 and 10 show the presence of intermediate depth seismicity (reddish dots in the maps on the left) under northern Taiwan. These events evidently reside in the subducted Philippine Sea plate whose western tip has been subducted under northern Taiwan (Wu et al., 2014). In profiles 1–3 of Figs. 8 the seismicity in western Taiwan is spare during this period, but the events near the tips of the arrows can be associated with those belonging to two layers, centered on 10 and 30–40 km (Wu et al., 1997, 2004, 2014). In all profiles in Fig. 8, there is a lack of earthquakes deeper than about 40 km under the high ranges. Seismicity under the southern Coastal Range, in eastern Taiwan, is dominated by a ~50° east-dipping zone (profiles 11–15, Figs. 8 and 10), associated with the well-known Chengkung thrust fault (Kuochen et al., 2007), but to the north Coastal Range seismicity structure is more complex.

The multitudinous small events show two previously unknown zones. In Figs. 8 and 10, a narrow seismic zone lies nearly inline with the mid-Taiwan transect (Fig. 3). These events are not in the CWB catalog and it is not a zone where there might be events of similar magnitude in the surrounding area that were not detected. These events define dipping zones in cross-sections (Fig. 10, profiles 7 and 8). The gently east-dipping zone at shallow depth may be viewed as a portion of the detachment, but the zone steepens rapidly to the east to reach 30 km (profiles 7 and 8, Fig. 10) and does not extend to the Central Range. The aftershocks of the two M > 6 events in 2013 (Chuang et al., 2013) define east-dipping zones in the vicinity of the deeper dipping zones in our results. Thus this 30–45° east-dipping zone can perhaps be viewed as a part of an active seismogenic fault. The other zone of interest lies in the part of the Central Range that has been relatively quiescent in terms of seismicity (Fig. 8 left, profile 6 in 8 right). It is limited to shallow depth (<10 km) and is sub-parallel to the boundary between the Cenozoic and older strata of the Central Range.

The array used in this study was not intended to provide uniform coverage of seismicity in Taiwan. The four linear arrays across the island and the two NS linear arrays at 5 km spacing surround the Central Range and provide better coverage than any former network largely because of station density. Combined with a robust algorithm for automatic

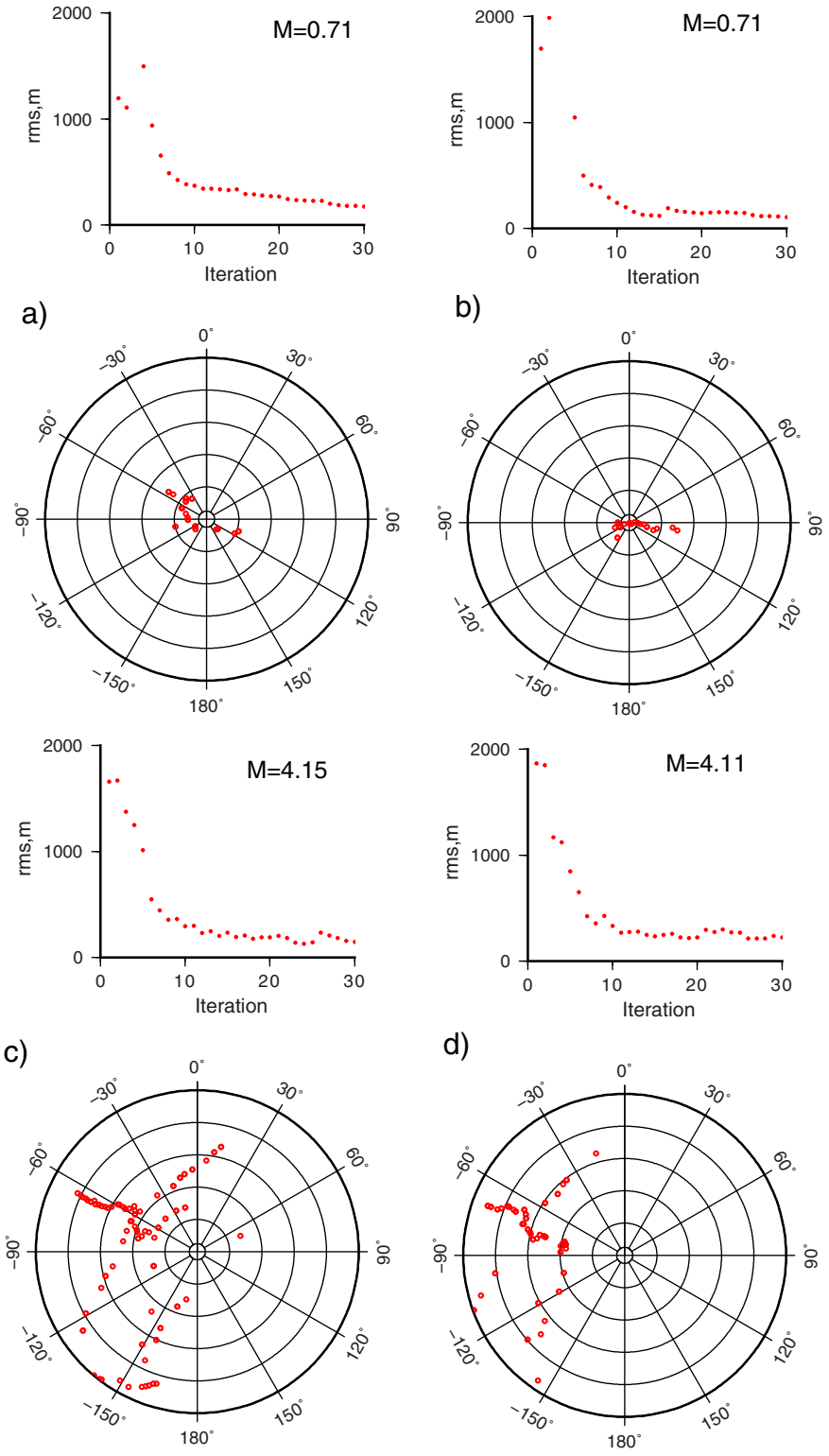

Fig. 11. RMS vs hypoDD iteration and azimuthal station coverage for four events. (a) and (b) Small events recorded by relatively few linearly distributed stations and both converge well. (c) M4.15 event with many more stations in eastern Central Range. (d) M4.11 offshore event with many stations but has a large "gap". For the convergence diagrams in each rms, in meters, are plotted against iteration number. In the polar station coverage diagrams the radial coordinate indicates station distance with each division at 20 km; only stations within 100 km to the epicenter is plotted.

detection, our catalog contains many more events at the low magnitude end than that of CWB (Fig. 12) as a result; given the strong spatial clustering of these events near the arrays (Fig. 6), one can imagine that many more events can be detected if additional stations were added between the arrays, or more practically, a series of dense arrays were used in local areas to supplement the permanent networks. As the terrain of

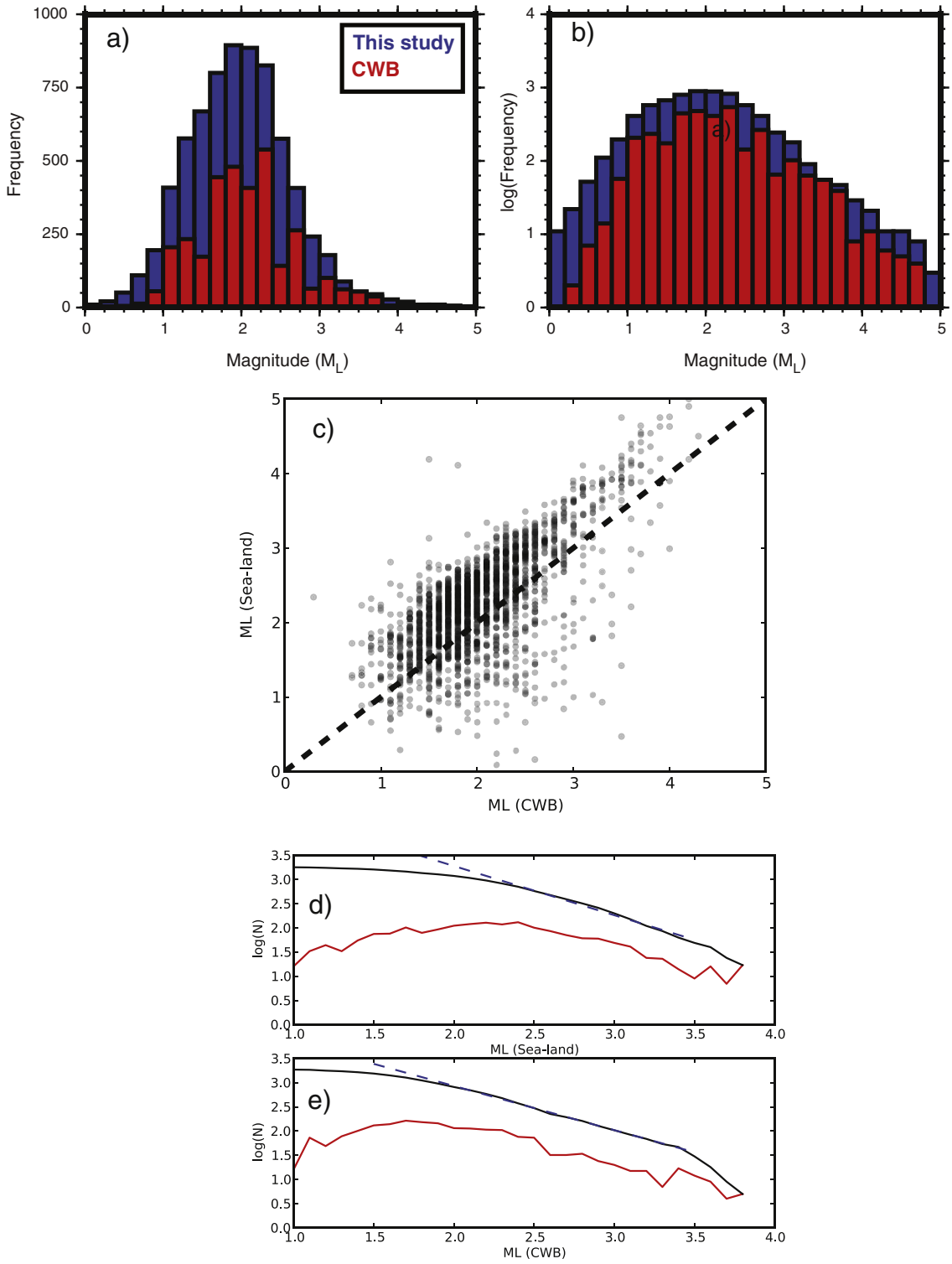

Fig. 12. (a) Comparison of the frequency-magnitude distributions between the TAIGER project (blue) and permanent national network (red) from 2009-03-20 to 2009-05-31. The left panel is in standard frequency units, (b) same plot with log N. Local magnitudes were calculated by simulating the Wood-Anderson frequency response. The TAIGER catalog has an estimated completeness magnitude of ML 2.1. Comparison with the CWB catalog indicates that some events between ML 2.5–3.0 were detected that are missing from the CWB catalog. The smallest magnitude events (ML 0–1) are greater in number by nearly an order of magnitude, or one full log unit. (c) M_L magnitudes for common events determined by CWB vs those determined in this work. (d) Comparison of frequency vs magnitude curves for TAIGER and (e) CWB events. (e) M_L magnitudes for common events determined by CWB vs those determined in this work.

the Central Range is rough, choices of station deployment were limited. As expected, when the maximum separation of events for clustering is progressively decreased in later iterations, the seismicity more clearly delineates possible fault structures. However, tight clustering does not imply better locations, as hypocenter scatters may be a reality. From a more practical standpoint, we use the results after 20 iterations

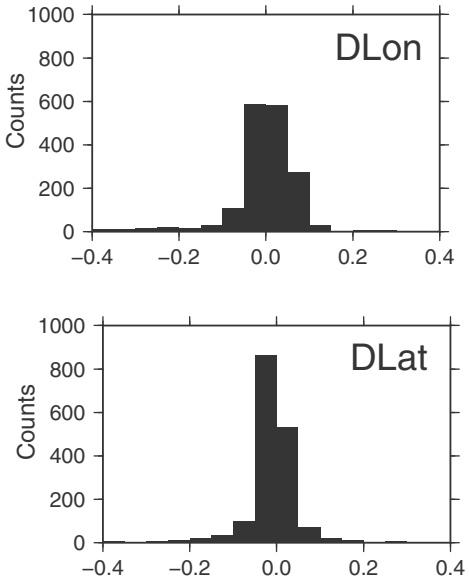

Fig. 13. Histograms of (top) longitudinal and (bottom) latitudinal offsets of CWB catalog from the results of our 20th iteration.

(Fig. 8) as a reference and those after 30 iterations (Fig. 10) to explore possible faults and their implications on tectonics. Better locations of some (especially offshore) events may be obtained by combining our data set with that of the CWB and southern Ryukyu stations.

Acknowledgment

We would like to acknowledge the support of NSF grants EAR0410227 and EAR1010645.

References

Allen, R.V., 1982. Automatic phase pickers: their present use and future prospects. Bull. Seismol. Soc. Am. 72 (6B), S225–S242.
Chuang, R.Y., Johnson, K.M., Wu, Y.-M., Ching, K.-E., Kuo, L.-C., 2013. A midcrustal ramp-fault structure beneath the Taiwan tectonic wedge illuminated by the 2013 Nantou earthquake series. Geophys. Res. Lett. 40, 5080–5084. http://dx.doi.org/10.1002/grl.51005.
Kennett, B.L.N., Engdahl, E.R., 1991. Traveltimes for global earthquake location and phase identification. Geophys. J. Int. 122, 429–465.
Kim, K.H., Chiu, J.M., Pujol, J., Chen, K.C., Huang, B.S., Yeh, Y.H., Shen, P., 2005. Three-dimensional VP and VS structural model associated with the active subduction and collision tectonics in the Taiwan region. Geophys. J. Int. 162, 204–220. http://dx.doi.org/10.1111/j.1365-246X.2005.02657.x.
Kuochen, H., Wu, Y.M., Chen, Y.G., Chen, R.Y., 2007. 2003 Mw6.8 Chengkung earthquake and its associated seismogenic structures. J. Asian Earth Sci. 31, 332–339.
Kuo-Chen, H., Wu, F., Chang, W.-L., Chang, C.-Y., Cheng, C.-Y., Hirata, N., 2015. Is the Lishan Fault of Taiwan active? Tectonophysics 661, 210–214.
Lee, Y.H., Chen, C.C., Liu, T.K., Ho, H.C., Lu, H.Y., Lo, W., 2006. Mountain building mechanisms in the Southern Central Range of the Taiwan Orogenic Belt—from accretionary wedge deformation to arc–continental collision. Earth Planet. Sci. Lett. 252, 413–422.
Pavlis, G.L., Vernon, F.L., Harvey, D., Quinlan, D., 2004. The generalized earthquake-location (GENLOC) package: an earthquake-location library. Comput. Geosci. 30, 9–10. http://dx.doi.org/10.1016/j.cageo.2004.06.010.
Ross, Z.E., Ben-Zion, Y., 2014a. An earthquake detection algorithm with pseudo probabilities of multiple indicators. Geophys. J. Int. 197, 458–463. http://dx.doi.org/10.1093/gji/ggt516.
Ross, Z.E., Ben-Zion, Y., 2014b. Automatic picking of direct P, S seismic phases and fault zone head waves. Geophys. J. Int. 199 (1), 368–381. http://dx.doi.org/10.1093/gji/ggu267.
Saragiotis, C.D., Hadjileontiadis, L.J., Panas, S., 2002. Pai–s/k: a robust automatic seismic P-phase arrival identification scheme. IEEE Trans. Geosci. Remote Sens. 40 (6), 1395–1404.
Seno, T., Stein, S., Gripp, A.E., 1993. A model for the motion of the Philippine Sea plate consistent with NUVEL-1 and geological data. J. Geophys. Res. 98. http://dx.doi.org/10.1029/93JB00782 (issn: 0148-0227).
Shin, T.C., Chen, Y.L., 1988. Study on the earthquake location of 3-D velocity structure in the Taiwan area. Meteorol. Bull. 42, 135–169.
Waldhauser, F., Ellsworth, W.L., 2000. A double-difference earthquake location algorithm: method and application to the northern Hayward Fault, California. Bull. Seismol. Soc. Am. 90 (6), 1353–1368.
Wang, C.Y., Shin, T.C., 1998. Illustrating 100 years of Taiwan seismicity. Terr. Atmos. Ocean. Sci. 9, 589–614.
Wu, F.T., Rau, R.J., Salzberg, D., 1997. Taiwan orogeny; thin-skinned or lithospheric collision? An introduction to active collision in Taiwan. Tectonophysics 274, 191–220.
Wu, F.T., Chang, C.S., Wu, Y.M., 2004. Precisely relocated hypocenters, focal mechanisms and active orogeny in Central Taiwan, aspects of the tectonic evolution of China. Geol. Soc. Lond. Spec. Publ. 226, 333–353.
Wu, F.T., Kuo-Chen, H., McIntosh, K.D., 2014. Subsurface imaging, TAIGER experiments and tectonic models of Taiwan. J. Asian Earth Sci. 90, 173–208. http://dx.doi.org/10.1016/j.jseaes.2014.03.024.

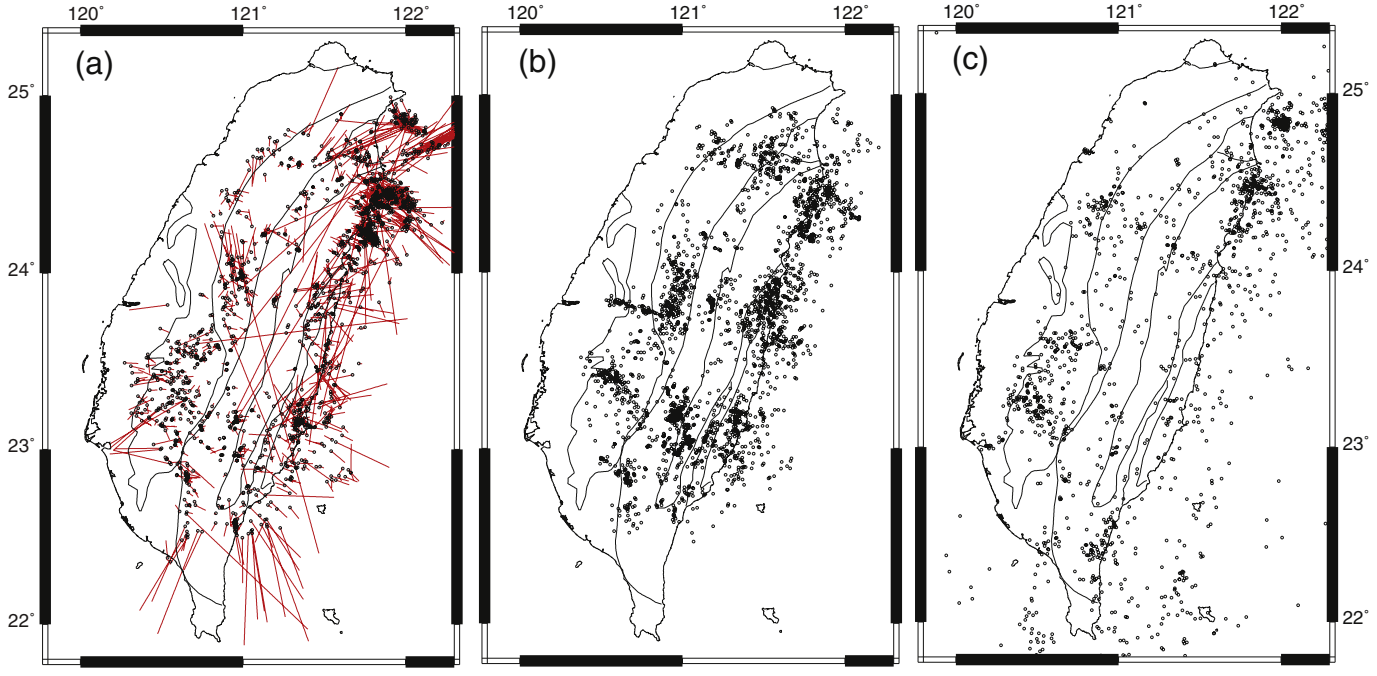

Fig. 14. Comparisons of auto-picking results and the CWB catalog events: (a) 1721 events contained in both catalogs from March 18 to May 31, 2009. Circles show our results and the end of the lines show locations of CWB events. (b) Events relocated in the 20th iteration of hypoDD that are not in the CWB catalog. (c) Events located by CWB but not in the TAIGER catalog.